Zak phase and the existence of edge states in graphene

P. Delplace
Département de Physique Théorique, Université de Genève, CH-1211 Genève, Switzerland

D. Ullmo
Laboratoire de Physique Théorique et Modèles Statistiques, CNRS UMR 8626, Univ. Paris-Sud, F-91405 Orsay Cedex, France

G. Montambaux
Laboratoire de Physique des Solides, CNRS UMR 8502, Univ. Paris-Sud, F-91405 Orsay Cedex, France
(Received 22 September 2011; revised manuscript received 30 October 2011; published 23 November 2011)

We develop a method to predict the existence of edge states in graphene ribbons for a large class of boundaries. This approach is based on the bulk-edge correspondence between the quantized value of the Zak phase $\mathcal{Z}(k_\parallel)$, which is a Berry phase across an appropriately chosen one-dimensional Brillouin zone, and the existence of a localized state of momentum $k_\parallel$ at the boundary of the ribbon. This bulk-edge correspondence is rigorously demonstrated for a one-dimensional toy model as well as for graphene ribbons with zigzag edges. The range of $k_\parallel$ for which edge states exist in a graphene ribbon is then calculated for arbitrary orientations of the edges. Finally, we show that the introduction of an anisotropy leads to a topological transition in terms of the Zak phase, which modifies the localization properties at the edges. Our approach gives a new geometrical understanding of edge states, and it confirms and generalizes the results of several previous works.

DOI: 10.1103/PhysRevB.84.195452 PACS number(s): 03.65.Vf, 73.22.Pr, 73.20.At

I. INTRODUCTION

The physics of edge states in two-dimensional (2D) systems has emerged as a very challenging problem in solid-state physics. A beautiful illustration occurs in graphene, a monolayer crystal of carbon,[1] where the existence of such states was predicted[2,3] in 1996 and confirmed experimentally later in graphene[4,5] and graphenelike structures.[6] This remarkable feature has led to strong research activity during the past few years. For instance, edge states were predicted to give rise to a novel type of magnetic ordering[2] and may lead to the realization of novel spintronic devices.[7,8]

In a broader context, edge states are also known to play an important role in quantum Hall systems[9,10] and topological insulators.[11,12] Because of their chiral character, the edge states in quantum Hall systems are robust against all kinds of disorders or interactions, while those in topological insulators survive scattering that preserves the time-reversal symmetry. This robustness against weak perturbations can be understood from a correspondence between the number of edge states and the value of a bulk topological number which is basically the Berry curvature integrated over the space of parameters, that is, the Brillouin zone of the 2D system.[12,13]

Edge states in graphene differ from those mentioned above, the most important distinction being that their existence depends on the boundary conditions fixed by the shape of the edge.[2,3] Two questions then naturally arise. The first one is related to the bulk-edge correspondence:[14–18] If the localization of a state at the edge depends on the boundaries, is it possible to relate its existence to a topological quantity defined within the bulk? The second question is simply whether we can predict the existence of edge states for an arbitrary type of edge (see, e.g., some examples in Fig. 1).

These two stimulating questions have already led to many works. In particular, Ryu and Hatsugai showed that edge states in 2D systems with chiral symmetry can be related to a bulk topological number defined in a reduced (1D) space of parameters.[14] More precisely, these authors were able to characterize edge states for three simple types of boundaries, namely the zigzag, armchair, and bearded edges (a bearded edge is a zigzag edge with dangling bonds, also called Klein defects).[19,20] Of course, even without disorder, there is an infinite number of different edge geometries in a honeycomb lattice, and several recent theoretical works addressed the existence of edge states for more sophisticated boundaries. Several of these works consist in tight-binding calculations of ribbon band structures.[2,3,21–23] A general study including many various shapes of edges was also conducted by Akhmerov and Beenakker.[24] Their work, performed within the continuous (Dirac) approximation, notably provides an analytical formula for the density of edge states.

The aim of this work is to precise the bulk-edge correspondence in graphene and to address a new method to predict the existence of edge states for a large class of edges. We show that it is possible to define in an unambiguous way a topological phase from the bulk Hamiltonian of graphene, which properly takes into account the shape of the edges. For a 1D system, this phase, called the Zak phase, is nothing but the integration of the Berry connection over the first Brillouin zone[25]

$$\mathcal{Z} = i \oint dq \langle u_q | \partial_q u_q \rangle, \tag{1}$$

where the $|u_q\rangle$ are the Bloch wave functions. In a 2D system, one difficulty is to define properly the path over which the integration is performed and to relate this quantity to the nature of the edge. In particular, for a translation invariant system in one direction, the Zak phase depends on the crystal momentum $k_\parallel$ associated with this direction. Here, we show that $\mathcal{Z}(k_\parallel)/\pi$ gives the number of states localized at the edge of the system.

The outline of the article is as follows. As the Zak phase is defined as a one-dimensional integral of the Berry

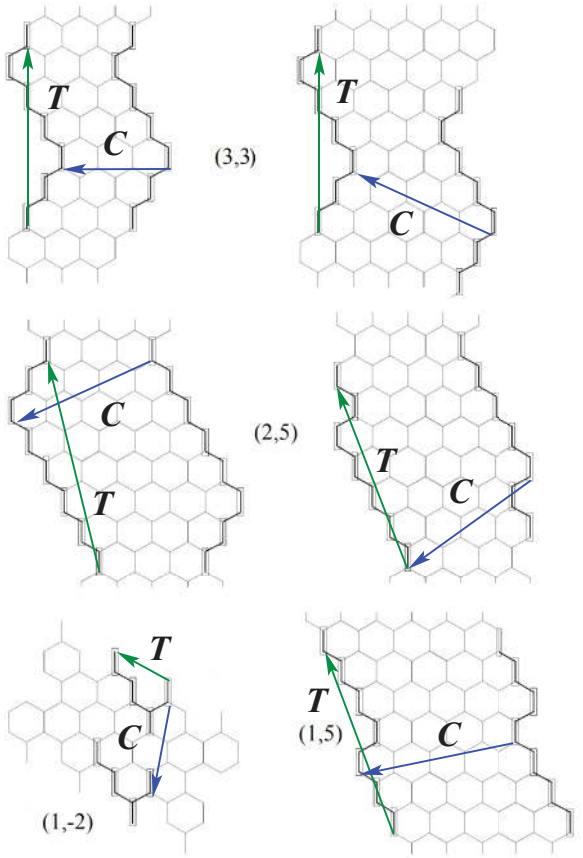

FIG. 1. (Color online) Examples of edges of different ribbons studied in this article. They are characterized by a translation vector $\mathbf{T}(m,n)$; see Sec. III B. The values of the couples (m,n) are specified in the figure. The edges of the ribbon $(1,-2)$ show dangling bounds since $mn < 0$. Different ribbons can be obtained from the same vector $\mathbf{T}(m,n)$ in two different ways. For instance, the lattice vectors $\mathbf{C}$ connecting the left and right edges of the two ribbons defined by $\mathbf{T}(3,3)$ differ. Another possibility is to draw a different "unit-cell" pattern for the same vector $\mathbf{T}$, as for the two ribbons defined by $\mathbf{T}(2,5)$.

connection, we first focus in Sec. II on a one-dimensional toy model for a chain of dimers. For this case, we give a simple demonstration of the bulk-edge correspondence between the Zak phase and the existence of edge states. Next, in Sec. III, we turn to graphene where a similar demonstration is performed for zigzag edges. By a formal analogy with the chain of dimers, we assume the generalization of this bulk-edge correspondence for the other boundaries. Then, we show how to define in an unambiguous way the Zak phase in graphene according to the nature of the edge and propose a very simple graphical method to evaluate it. This information then directly gives us the range of $k_\parallel$ for which edge states exist. The analytical results are in perfect agreement with those of Akhmerov and Beenakker[24] and reproduce many numerical works. Finally, in Sec. IV, we extend our approach by considering nonequal hopping parameters in the honeycomb lattice. We discuss the existence of edge states in this case and explain recent numerical calculations in terms of the Zak phase.[26]

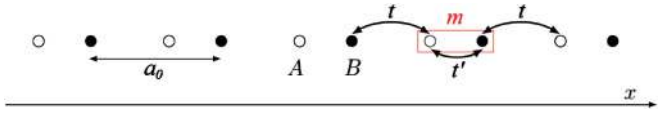

FIG. 2. (Color online) Chain of dimers A-B. The chain starts with an atom A and ends with an atom B. t and t' are the hopping parameters and a_0 is the lattice spacing. The unit cell m is represented by a rectangle.

II. THE ZAK PHASE AND THE EDGE STATES IN THE CHAIN OF DIMERS

To illustrate the relation between the Zak phase and boundary states, we consider in this section a simple model, a one-dimensional chain of dimers A-B as shown in Fig. 2. The two atoms of the dimers are coupled by a hopping parameter t' and the chain is obtained by coupling periodically the dimers with a hopping parameter t. The lattice spacing (between two consecutive identical atoms) is a_0.

The aim of this section is to show in a simple way that the Zak phase $\mathcal{Z}$ is governed by the ratio t'/t and that the topological transition $(\mathcal{Z}=0) \to (\mathcal{Z}=\pi)$ corresponds to the emergence of edge states in the finite system.

A. The bulk Hamiltonian

The Hamiltonian of the dimer chain is given by

$$\hat{H} = \sum_{m=1}^{M} t' b_m^\dagger a_m + t a_{m+1}^\dagger b_m + \text{H.c.}, \tag{2}$$

where $a_m^\dagger$ (respectively $b_m^\dagger$) creates a particle on the site A (respectively B) of the mth dimer.

For periodic boundary conditions, we can use the Bloch theorem and rewrite $\hat{H}$ as

$$\hat{H} = \sum_{k_n \equiv \frac{2\pi n}{a_0}} \Psi_{k_n}^\dagger \mathcal{H}^B(k_n) \Psi_{k_n} \qquad \left(-\frac{M}{2} < n < \frac{M}{2}\right), \tag{3}$$

with $\Psi_k^\dagger = (\psi_{A,k}^\dagger, \psi_{B,k}^\dagger) = M^{-1/2} \sum_{m=1}^{M} e^{i a_0 m k} (a_m^\dagger, b_m^\dagger)$ and

$$\mathcal{H}^B(k) = -t \begin{bmatrix} 0 & \rho(k) \\ \rho^*(k) & 0 \end{bmatrix}, \tag{4}$$

where $\rho(k) = t'/t + e^{-ika_0}$. Introducing $\sigma = (\sigma_x, \sigma_y)$ the vector of Pauli matrices, $\mathcal{H}^B(k)$ can be expressed in the form

$$\mathcal{H}^B(k) = -t\, \mathbf{g}(k) \cdot \sigma, \tag{5}$$

with $\mathbf{g}(k) = (\mathbb{R}e\ \rho, -\mathbb{I}m\ \rho) = (t'/t + \cos ka_0, \sin ka_0)$. Diagonalizing $\mathcal{H}^B(k)$ we obtain the eigenvalues

$$\begin{aligned} \epsilon_{k,\pm} &= \pm t\, |\mathbf{g}(k)| = \pm t\, |\rho(k)| \\ &= \pm \sqrt{t^2 + t'^2 + 2tt' \cos(ka_0)}, \end{aligned} \tag{6}$$

and writing $\rho(k) = |\rho(k)| e^{-i\phi(k)}$, we have

$$\mathbf{g}(k) = |\rho(k)| \begin{bmatrix} \cos\phi(k) \\ \sin\phi(k) \end{bmatrix}, \tag{7}$$

with the phase $\phi(k)$ given by

$$\cot\phi(k) = \frac{t'/t}{\sin ka_0} + \cot ka_0. \tag{8}$$

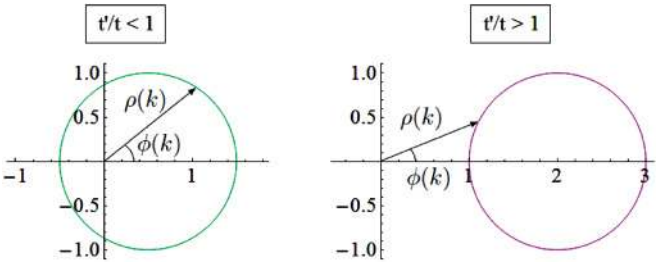

FIG. 3. (Color online) Two trajectories of the vector $\mathbf{g}(k)$ with different topologies when k runs across the Brillouin zone. When $t'/t < 1$ ($t'/t > 1$) the curve $\mathbf{g}(k)$ does (not) wind around the origin.

The winding of the vector $\mathbf{g}(k)$ as k varies across the Brillouin zone is shown in Fig. 3 for two values of t'/t. When $t'/t > 1$, the curve $\mathbf{g}(k)$ does not enclose the origin and $|\phi(k)| < \pi/2$ for all k. When $t'/t < 1$, the loop encloses the origin and the phase $\phi(k)$ can take any value. This topological behavior of the phase $\phi(k)$ is, furthermore, closely related to the value of the Zak phase. Indeed, the eigenvectors of $\mathcal{H}^B(k)$ are of the form

$$|u_{k,\pm}\rangle = \frac{1}{\sqrt{2}}\begin{pmatrix} e^{-i\phi(k)} \\ \pm 1 \end{pmatrix}, \tag{9}$$

and the definition Eq. (1) of the Zak phase gives

$$\mathcal{Z} = \frac{1}{2}\oint dk \frac{d\phi}{dk} = \frac{\Delta\phi}{2}, \tag{10}$$

where $\Delta\phi$ is the variation of $\phi(k)$ when k varies across the full Brillouin zone. The Zak phase $\mathcal{Z}$ is π times the winding number of the curve $\mathbf{g}(k)$ around the origin and is, therefore, zero if this curve does not enclose the origin and π if it does. Thus,

$$\begin{aligned} \mathcal{Z} &= 0 \quad \text{when} \quad t'/t > 1 \\ \mathcal{Z} &= \pi \quad \text{when} \quad t'/t < 1. \end{aligned} \tag{11}$$

Equation (11) shows that tuning the ratio t'/t induces a topological transition (at $t'/t = 1$) characterized by the Zak phase $\mathcal{Z} = 0 \longleftrightarrow \mathcal{Z} = \pi$.

B. Open boundary conditions

1. The missing bulk states and the Zak phase

Consider now a finite chain of M dimers with open boundary conditions. We impose that the wave function vanishes at the nearest site outside the chain, that is, on the B site at $m = 0$ and the A site at $m = (M + 1)$. Most of the eigenvectors can be constructed as linear combinations $|v_{k,\pm}\rangle$ of the bulk eigenfunctions with opposite momentum $|u_{k,\pm}\rangle$ and $|u_{-k,\pm}\rangle$. Writing $|u_{k,\pm}\rangle$ as

$$|u_{k,\pm}\rangle = \sqrt{\frac{1}{2M}}\sum_{m=1}^{M} e^{ika_0 m}\begin{pmatrix} e^{-i\phi(k)} \\ \pm 1 \end{pmatrix}(|m,A\rangle, |m,B\rangle), \tag{12}$$

where $|m, A/B\rangle$ denotes the orbital A/B in the cell m, we obtain from the condition $\langle 0, B|v_{k,\pm}\rangle = 0$ that $|v_{k,\pm}\rangle = \frac{1}{\sqrt{2}}[|u_{k,\pm}\rangle - |u_{-k,\pm}\rangle]$. Thus, using $\phi(-k) = -\phi(k)$, we have

$$|v_{k,\pm}\rangle = \frac{i}{\sqrt{M}}\sum_{m}\begin{bmatrix} \sin[ka_0 m - \phi(k)] \\ \pm \sin(ka_0 m) \end{bmatrix}(|m,A\rangle, |m,B\rangle). \tag{13}$$

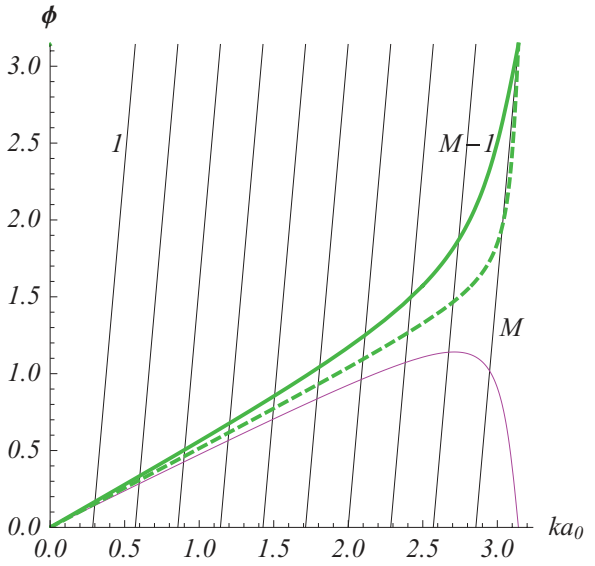

FIG. 4. (Color online) Variation $\phi(k)$ for $t'/t = 1.1$ (bottom curve), $t'/t = 0.8$ (upper thick curve), and $t'/t = 0.95$ (thick dashed curve). The straight lines are lines of equation $f_\kappa(k) = (M + 1)ka_0 - \kappa\pi$. Here, we have chosen $M = 10$, for which $(t'/t)_c = 0.9091$. The extreme values of κ are indicated on the figure. In the latter case $t'/t = 0.95 > (t'/t)_c$, so there are M bulk states although the Zak phase $\mathcal{Z} = \pi$.

Finally, the boundary condition $\langle (M + 1), A|v_{k,\pm}\rangle = 0$ imposes the quantization condition

$$k(M + 1)a_0 - \phi(k) = \kappa\pi, \qquad \kappa = 1, \ldots, M, \tag{14}$$

which has to be solved in the range $0 < k < \pi/a_0$ (the wave functions corresponding to $k = 0$ and $k = \pi/a_0$ are identically zero). The function $\phi(k)$ is plotted in Fig. 4, and the solutions of Eq. (14) correspond to the intersection of $\phi(k)$ with the M lines $f_\kappa(k) = (M + 1)ka_0 - \kappa\pi$.

From this figure, we see that the Zak phase controls the number of bulk states and, therefore, the existence of edge states. Indeed, when $t' > t$, $\phi(\pi/a_0) = 0$ and Eq. (14) has M solutions. When $t' < t$, $\phi(\pi/a_0) = \pi$ and in this case there are M or $M - 1$ solutions depending on the value of t'/t. By comparing the slopes of the curves $\phi(k)$ and $f_M(k)$, we immediately obtain that the number of bulk states $|v_{k,\pm}\rangle$ depends on the critical value of the ratio t'/t

$$\left(\frac{t'}{t}\right)_c = 1 - \frac{1}{M + 1}. \tag{15}$$

Including the factor 2 associated with negative and positive energies for each solution of the quantization condition (14), the number N_{bulk} of bulk states is:

$$\begin{aligned} N_{\text{bulk}} &= 2M \qquad \text{when} \quad t'/t > (t'/t)_c \\ N_{\text{bulk}} &= 2(M - 1) \quad \text{when} \quad t'/t < (t'/t)_c. \end{aligned} \tag{16}$$

As we show below, the missing states are edge states localized at the ends of the chain. In the large M limit, the number of bulk states is related to the value of $\phi(\pi/a_0)$ since, in this limit, there are $2M$ bulk solutions when $\phi(\pi/a) = 0$ and $2(M - 1)$ bulk solutions when $\phi(\pi/a) = \pi$. This criterion can be rewritten in

terms of the Zak phase: Since $\phi(k)$ is an odd function of k, we have simply

$$\mathcal{Z} = \frac{1}{2}\oint dk \frac{d\phi}{dk} = \int_0^{\pi/a_0} dk \frac{d\phi}{dk} = \phi(\pi/a_0) = 0 \text{ or } \pi. \quad (17)$$

As a result, by comparing Eqs. (11), (15), and (16), we conclude that in the large M limit,[27]

$$\begin{aligned} N_{\text{bulk}} &= 2M \qquad \text{when} \quad \mathcal{Z} = 0 \\ N_{\text{bulk}} &= 2(M-1) \qquad \text{when} \quad \mathcal{Z} = \pi. \end{aligned} \quad (18)$$

2. The edge states

We now briefly describe the structure of the edge state for $t'/t < (t'/t)_c$. We search for a solution k of the form $k = \pi/a_0 + i\lambda$, where $\xi = 1/\lambda$ is the localization length of the edge state. The solution vanishing on the B site at $m = 0$ is of the form

$$|v^e_{\lambda,\pm}\rangle = \frac{1}{\sqrt{M}} \sum_{m=1}^{M} (-1)^{m+1} \begin{pmatrix} \chi^A_m \\ \chi^B_m \end{pmatrix} (|m,A\rangle, |m,B\rangle), \quad (19)$$

where

$$\begin{pmatrix} \chi^A_m \\ \chi^B_m \end{pmatrix} = \begin{Bmatrix} \left[\frac{t'}{t}\sinh\lambda a_0 m - \sinh\lambda a_0(m-1)\right]/|\rho(\lambda)| \\ \pm \sinh\lambda a_0 m \end{Bmatrix}, \quad (20)$$

and has an energy

$$\epsilon_{\lambda,\pm} = \pm\sqrt{t^2 + t'^2 - 2tt'\cosh\lambda a_0} \equiv \pm t\ |\rho(\lambda)|. \quad (21)$$

The inverse localization length λ is fixed by the condition that the wave function on the site A at $m = (M+1)$ vanishes, leading to

$$t' \sinh\lambda(M+1)a_0 = t \sinh\lambda M a_0. \quad (22)$$

Inserting (22) into (21), we find

$$\epsilon_{\lambda,\pm} = \pm t \frac{\sinh\lambda a_0}{\sinh\lambda(M+1)a_0}, \quad (23)$$

and the components of the edge states wave functions can be rewritten as

$$\begin{pmatrix} \chi^A_m \\ \chi^B_m \end{pmatrix} = \begin{bmatrix} \sinh\lambda a_0(M+1-m) \\ \pm \sinh\lambda a_0 m \end{bmatrix}, \quad (24)$$

which satisfy properly the boundary conditions. Far from the transition, that is, when the localization length $\xi = 1/\lambda$ is much smaller than the size of the chain Ma_0, Eq. (22) reads

$$\frac{t'}{t} \simeq \exp(-\lambda a_0). \quad (25)$$

This implies $\cosh(\lambda a_0) \simeq (t^2 + t'^2)/2tt'$ and, thus ,$\epsilon_{\lambda,\pm} \simeq 0$. More precisely, from Eq. (23), the energy vanishes as $\epsilon_{\lambda,\pm} \simeq \exp(-\lambda M a_0)$. The dependence $\lambda(t'/t)$ for a chain of $M = 10$ dimers is shown in Fig. 5, together with the approximate expression Eq. (25). The energy spectrum of the same chain is displayed in Fig. 6.

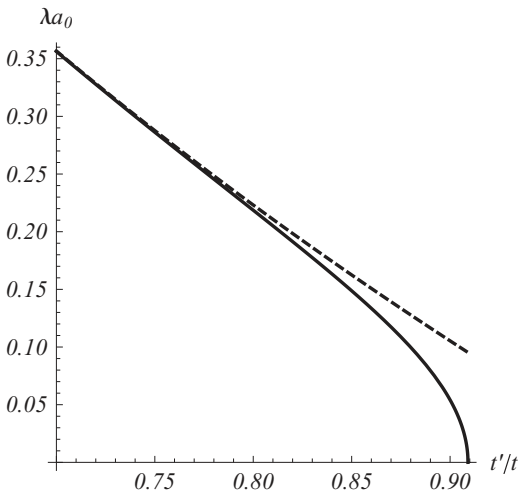

FIG. 5. Inverse localization length λ as a function of the parameter t'/t, for a chain of $M = 10$ dimers. The full curve is the solution of Eq. (22). As expected, it diverges as the ratio t/t' reaches the critical value given by Eq. (15). The dashed line corresponds to the approximation (25) valid far from the transition and corresponding to $\epsilon = 0$.

C. Remarks on the chiral symmetry

We finish this section with a few brief remarks concerning the Zak phase and symmetries. As first stressed by Ryu and Hatsugai,[14] the fact that the edge states have zero energy is associated with the existence of a chiral symmetry of the bulk Hamiltonian.[28] From an algebraic point of view, a chiral symmetry is represented by an operator $\mathcal{C}$ that anticommutes with the bulk Hamiltonian and that satisfies $\mathcal{C}^2 = \mathbb{1}$. As the Bloch Hamiltonian of the chain of dimers can be written as a linear combination of the Pauli matrices σ_x and σ_y, it

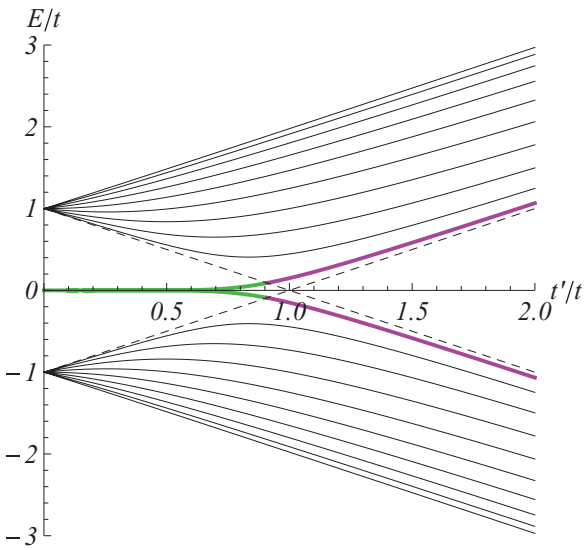

FIG. 6. (Color online) Energy levels as a function of the parameter t'/t, for a chain of $M = 10$ dimers. There is an edge state with an energy close to 0 when $t'/t < 1 - 1/(1+M)$. The dashed lines correspond to the gap $\pm(t'-t)$ in the limit $M \to \infty$. The thick (light-purple) curve is the energy of the lowest energy state, which becomes an edge state (light-green curve) when $t'/t < (t'/t)_c$.

is clear that $\mathcal{C} = \sigma_z$ fulfills these properties. We now note that the Zak phase measures the solid angle drawn by the pseudospinor in the Bloch sphere when k spans the Brillouin zone. As long as the Hamiltonian does not have a component proportional to σ_z, the pseudospinor is forced to evolve on the equator of the Bloch sphere, and the Zak phase is necessarily a multiple of π. We note that breaking the inversion symmetry of the chain,[25] for instance, by adding a staggered potential, would add a term proportional to σ_z in the Hamiltonian and, therefore, would break the chiral symmetry. As a consequence, the Zak phase is no longer expected to be a multiple of π in this case and the energy of the edge states can differ from zero.

Adding a term proportional to the identity trivially breaks the chiral symmetry and shifts the energy while leaving the pseudospinor on the equator so the Zak phase is still quantized as a multiple of π. A configuration where this simple mechanism leads to an interesting physics is obtained by coupling chains of dimers (assumed oriented along the x direction) by a hopping parameter t'' along the y direction, as displayed in Fig. 7.

For periodic boundary conditions, the bulk Hamiltonian of the coupled chains reads

$$\mathcal{H}^B_{cc} = -t'' \cos(k_y b_0)\mathbb{1} + \mathcal{H}^B, \tag{26}$$

with b_0 the distance between two chains. We see that the term proportional to $\mathbb{1}$ involves a dispersion along the y direction and does not change the properties of the Zak phase which are encoded in $\mathcal{H}^B$. Therefore, two distinct topological phases ($\mathcal{Z} = 0$ and $\mathcal{Z} = \pi$) arise when the criteria given in Eq. (16) is satisfied. This means that when $\mathcal{Z} = \pi$, a ribbon of finite width in the x direction and invariant by translation in the y direction supports dispersive edge states along its edges, as shown in Fig 8.

This example shows that the Zak phase may help characterizing the edge states even in the absence of a chiral symmetry. In addition, it also illustrates that the Zak phase, which until now we have defined for a one-dimensional system, may provide informations about the edge states in systems of higher dimension. In the following of the paper, we investigate the more complex case of a monolayer of graphene.

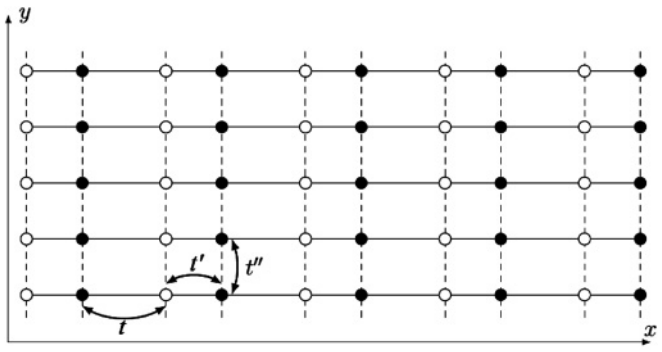

FIG. 7. Chains of dimers coupled in the y direction by a hopping parameter t''.

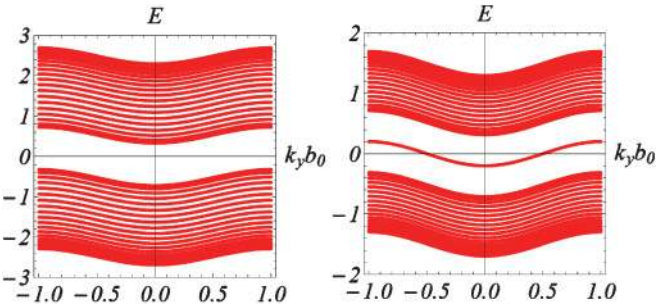

FIG. 8. (Color online) Energy levels of a ribbon built from chains of $M = 20$ dimers. The chains are coupled to one other in the y direction with a hopping parameter $t'' = 0.1$, and the ribbon is invariant by translation along this direction. We took $t = 1$, (left) $t' = 1{,}5$, and (right) $t' = 0{,}5$. In the first case the Zak phase is $\mathcal{Z} = 0$ and there is no edge state. In the other case, the Zak phase is $\mathcal{Z} = \pi$ and dispersive edge states have emerged in the gap.

III. THE ZAK PHASE AND THE EDGE STATES OF GRAPHENE RIBBONS

Turning now to graphene, we demonstrate in this section that the Zak phase, introduced in Sec. II for a one-dimensional system, has a natural generalization for a large class of two-dimensional graphene ribbons. In the particular case of zigzag edges, following the same lines as in the 1D case, we prove that it is possible to relate the Zak phase to the existence of edge states. We then consider the case of ribbons with arbitrary orientations and show that, computing the Zak phase, we can predict the presence or absence of edge states according to the nature of the edge.

A. The bulk Hamiltonian

We describe the electronic spectrum of graphene by a tight-binding model on the triangular Bravais lattice with two atoms (A and B) per unit cell, as illustrated in Fig. 9. The parameters t_1, t_2, and t_3 represent the three hopping integrals between nearest neighbors and for now we consider the isotropic case $t_1 = t_2 = t_3$ (the anisotropic case is treated in Sec. IV). The vectors $\mathbf{a}_1$ and $\mathbf{a}_2$ form a basis of the Bravais lattice, and we note $(\mathbf{a}_1^*, \mathbf{a}_2^*)$ (with $\mathbf{a}_i^* \cdot \mathbf{a}_j = 2\pi\delta_{ij}$) the associated basis of the reciprocal space.

For periodic boundary conditions in both the x and y directions, Bloch theorem leads to the bulk Hamiltonian

$$H^B(\mathbf{k}) = -t_3|\rho(\mathbf{k})| \begin{pmatrix} 0 & e^{-i\phi(\mathbf{k})} \\ e^{i\phi(\mathbf{k})} & 0 \end{pmatrix} \tag{27}$$

in the basis of the two sublattices A and B, with

$$\begin{aligned} \rho(\mathbf{k}) &= 1 + \frac{t_1}{t_3}\exp(-i\mathbf{k}\cdot\mathbf{a}_1) + \frac{t_2}{t_3}\exp(-i\mathbf{k}\cdot\mathbf{a}_2) \\ &= |\rho(\mathbf{k})|e^{-i\phi(\mathbf{k})}. \end{aligned} \tag{28}$$

The eigenenergies of the bulk Hamiltonian $H^B(\mathbf{k})$ consist in two bands, given by $\epsilon_\pm(\mathbf{k}) = \pm t_3|\rho(\mathbf{k})|$, and the corresponding eigenvectors have the form,

$$|u_{\mathbf{k},\pm}\rangle = \frac{1}{\sqrt{2}} \begin{pmatrix} e^{-i\phi(\mathbf{k})} \\ \pm 1 \end{pmatrix}. \tag{29}$$

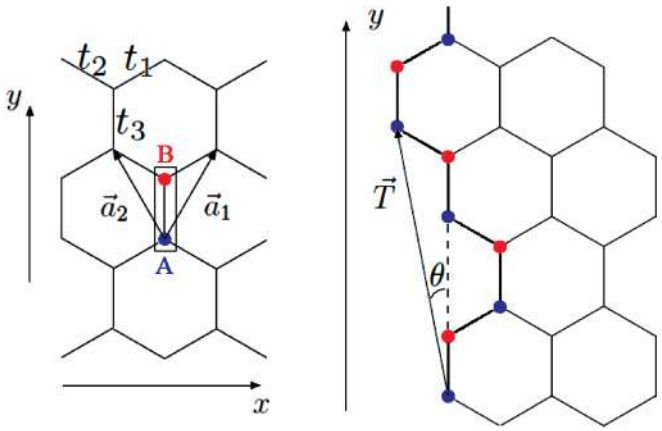

FIG. 9. (Color online) (Left) Unit cell (dimer) A-B of the graphene sheet with the basis vectors of the Bravais lattice $\mathbf{a}_1$ and $\mathbf{a}_2$ and the hopping parameters t_1, t_2, and t_3. (Right) Example of an edge obtained by translating the dimer along $\mathbf{a}_1$ and then twice along $\mathbf{a}_2$. This edge is characterized by the periodicity vector $\mathbf{T} = \mathbf{a}_1 + 2\mathbf{a}_2$.

The positive and negative bands touch linearly at two inequivalent points $\mathbf{D}$ and $\mathbf{D}'$ (the Dirac points) which, in the isotropic case considered in this section, are located at the corners $\mathbf{K}$ and $\mathbf{K}'$ of the first Brillouin zone.

The Hamiltonian (27) can be written in the same form $H^B(\mathbf{k}) = -t_3\ \mathbf{g}(\mathbf{k}) \cdot \sigma$ as for the chain of dimers (5), the difference being that $\mathbf{k}$ is now a two-dimensional vector and that the $\mathbf{k}$ dependence of $\mathbf{g}(\mathbf{k})$ is, of course, not the same. As in our 1D toy model, topological properties of the wave function as well as some characterization of the edge states are expected to be encoded in the loops drawn by $\mathbf{g}(\mathbf{k})$ as $\mathbf{k}$ varies across the Brillouin zone. This connection was actually already suggested by Ryu and Hatsugai[14] in the broader context of systems with chiral symmetry (and more recently by Mong and Shivamoggi in a general study of Dirac Hamiltonians).[15] Their approach, which basically consists in the graphical evaluation of the Zak phase in the same way as in Fig. 3, was applied for three different regular types of edges (zigzag, armchair, and bearded edges). Comparing with numerical calculations, they showed that the Zak phase could correctly predict the existence of edge states in these cases. However, their approach relied on the construction of a *specific* bulk Hamiltonian [i.e., a vector $\mathbf{g}(\mathbf{k})$] for each type of edge considered and is, therefore, not convenient to consider arbitrary boundary conditions. Here, we keep the *same* bulk Hamiltonian but we associate a *specific* 2D Brillouin zone to each type of edge. This allows us to predict the existence of edge states for different ribbon geometries and, therefore, to address a significantly larger class of ribbons.

B. Edges of graphene ribbons

Turning now to graphene ribbons, we assume that both edges of the ribbon are parallel (i.e., that one edge can be deduced from the other by translation of a lattice vector $\mathbf{C}$) and constructed as illustrated in Fig. 9, i.e., by connecting dimers A-B (or unit cells) *of fixed orientation* (vertical orientation in Fig. 9).

More precisely, considering two positive or negative integers m and n, an edge is built as $(|m| + |n|)$ translations of the dimer, $|m|$ of which are along $\mathbf{a}_1$ ($-\mathbf{a}_1$ if m negative) and $|n|$ of which are along $\mathbf{a}_2$ ($-\mathbf{a}_2$ if n negative), in an arbitrary order, and by repeating the pattern obtained in this way. Therefore, the edges are invariant under the translation vector $\mathbf{T} = m\mathbf{a}_1 + n\mathbf{a}_2$ which characterizes the type of edge. Noting θ the angle between $\mathbf{T}$ and the y axis, this angle is related to (m,n) through

$$\tan\theta = \frac{1}{\sqrt{3}}\frac{n-m}{n+m}. \tag{30}$$

When m and n have the same sign, the class of edges constructed in this way exactly corresponds to the "minimal boundary conditions" defined by Akhmerov and Beenakker.[24] In the other case, the edges exhibit dangling bonds. Figure 1 gives some examples of such edges. It is easy to see that the vectors $\mathbf{T}(m,n)$ and $\mathbf{T}(n,m)$ describe the same kind of edge. We also notice that the same vector $\mathbf{T}$ can describe edges with different shapes; see the example of $\mathbf{T} = (2,5)$ in Fig. 1.

We stress that choosing the "unit-cell" dimer A-B with a different orientation (i.e., rotated from $\pm 2\pi/3$ with respect to the vertical one used in Fig. 9) leads to a different set of boundaries. These latter are, of course, just deduced from the former by a $\pm 2\pi/3$ rotation, and, thus, considering only the vertical unit-cell dimer, as we shall do in the following, does not restrict the type of edge to be studied. We insist, however, that if one wanted to consider another orientation of the unit-cell dimer for the edges, it would be essential to *modify accordingly the dimer orientation* in the definition of the *bulk* Hamiltonian [which basically fixes the zero of the phase $\phi(\mathbf{k})$ in Eqs. (27) or (29)]. This is a necessary condition to derive a bulk-edge correspondence for the edge states in terms of the Zak phase.

C. The Zak phase in graphene ribbons

For one-dimensional models such as the one considered in Sec. II, the Zak phase is defined as the integral of the Berry connection across the Brillouin zone. To generalize this notion to two-dimensional systems such as graphene, this integration should be taken on a cut of a 2D Brillouin zone in a direction transverse to the ribbon orientation. More precisely, as the ribbon is assumed to be invariant under translation by the vector $\mathbf{T}$, Bloch theorem guarantees that $k_\parallel$, the component of the crystal momentum parallel to $\mathbf{T}$, is a good quantum number. We expect, therefore, the Zak phase $\mathcal{Z}(k_\parallel)$ to be a function of $k_\parallel$ and to correspond to an integration of the Berry connection across the 2D Brillouin zone along a perpendicular direction $k_\perp$.

Let us assume for now that m and n are coprime integers (we will return below to the case where they are not). We choose the Brillouin zone from which the Zak phase will be computed as the one generated by two orthogonal vectors of the reciprocal space, $\mathbf{\Gamma}_\parallel$ and $\mathbf{\Gamma}_\perp$, obtained as follows. The first of these vector $\mathbf{\Gamma}_\parallel \equiv 2\pi\mathbf{T}/|\mathbf{T}|^2$ is parallel to the direction $\mathbf{T}$ of the ribbon and merely defines the one-dimensional Brillouin zone of the ribbon. The second vector $\mathbf{\Gamma}_\perp$ is taken perpendicular to $\mathbf{T}$, and its norm is fixed by the constraint that $\mathbf{\Gamma}_\parallel \times \mathbf{\Gamma}_\perp = \mathbf{a}_1^* \times \mathbf{a}_2^*$ (where, as mentioned above, $\mathbf{a}_1^*$ and $\mathbf{a}_2^*$ are the reciprocal lattice

vectors defined by $\mathbf{a}_i \cdot \mathbf{a}_j^* = 2\pi\delta_{ij}$). This leads to

$$\mathbf{\Gamma}_\parallel(m,n) = \frac{(n+2m)\mathbf{a}_1^* + (m+2n)\mathbf{a}_2^*}{2(n^2+m^2+nm)} \tag{31}$$

$$\mathbf{\Gamma}_\perp(m,n) = n\mathbf{a}_1^* - m\mathbf{a}_2^*. \tag{32}$$

For the sake of completeness we remind briefly in Appendix why $(\mathbf{\Gamma}_\parallel,\mathbf{\Gamma}_\perp)$ constructed in this way actually defines a Brillouin zone when (m,n) are coprime integers (and only in this case).

For an arbitrary edge characterized by the vector $\mathbf{T}(m,n)$, we introduce the unit vectors $\mathbf{e}_\parallel = \mathbf{\Gamma}_\parallel/|\mathbf{\Gamma}_\parallel|$ and $\mathbf{e}_\perp = \mathbf{\Gamma}_\perp/|\mathbf{\Gamma}_\perp|$ and write the momentum as $\mathbf{k} = k_\parallel\mathbf{e}_\parallel + k_\perp\mathbf{e}_\perp$. The Zak phase $\mathcal{Z}(k_\parallel)$ can thus be defined as:

$$\mathcal{Z}(k_\parallel) = i\oint dk_\perp \langle u_{\mathbf{k},\pm}|\partial_{k_\perp} u_{\mathbf{k},\pm}\rangle, \tag{33}$$

which, by using the expression of the Bloch function (29), simply reads

$$\mathcal{Z}(k_\parallel) = \frac{1}{2}\oint dk_\perp \partial_{k_\perp}\phi(\mathbf{k}). \tag{34}$$

Note that as $\mathbf{\Gamma}_\perp$ is a vector of the reciprocal lattice, the integration can indeed be seen as taken on a closed path.

Let us consider now the situation where m and n are not coprime, in which case $(\mathbf{\Gamma}_\parallel,\mathbf{\Gamma}_\perp)$ obtained from Eqs. (31) and (32) do not form a basis of the reciprocal lattice (see Appendix). Writing $m = l\tilde{m}$ and $n = l\tilde{n}$ with l integer and $\tilde{m}$ and $\tilde{n}$ coprime and following exactly the same line of argument as above, we can construct a basis $(\tilde{\mathbf{\Gamma}}_\parallel,\tilde{\mathbf{\Gamma}}_\perp)$ of the reciprocal lattice corresponding to $(\tilde{m},\tilde{n})$ and define the Zak phase $\mathcal{Z}_{(\tilde{m},\tilde{n})}(\tilde{k}_\parallel)$ accordingly from Eq. (34). An example of such a construction will be shown in Sec. III E [see the case $(m,n) = (2,0)$ in Fig. 13]. However, as $\mathbf{T}(\tilde{m},\tilde{n}) = \mathbf{T}(m,n)/l$, we now have $\tilde{\mathbf{\Gamma}}_\parallel = l\mathbf{\Gamma}_\parallel$. As a consequence, to a given value $k_\parallel$ of the quantum number of the ribbon corresponds l values $(\tilde{k}_\parallel^{(0)},\ldots,\tilde{k}_\parallel^{(l-1)})$ in the Brillouin zone $(\tilde{k}_\parallel^{(j)} = k_\parallel + j|\tilde{\mathbf{\Gamma}}_\parallel|)$ and, therefore, l Zak phases. The prescription we shall use for noncoprime integers (m,n) is, therefore, that, for a given value $k_\parallel$ of the ribbon quantum number, the Zak phase is defined as

$$\mathcal{Z}_{(m,n)}(k_\parallel) \equiv \sum_{j=1}^{l} \mathcal{Z}_{(\tilde{m},\tilde{n})}(\tilde{k}_\parallel^{(j)}). \tag{35}$$

This prescription merely corresponds to a folding of the Brillouin zone.

D. Zigzag boundary conditions

Before we address general orientations for the graphene ribbon, let us, first, consider in detail the simple case of zigzag boundary conditions. In that case, and as illustrated in Fig. 10, the two edges of the ribbon, $(\boldsymbol{\beta}_1)$ and $(\boldsymbol{\beta}_2)$, are constructed as the vertical dimer A-B translated periodically with the vector $\mathbf{T} = \mathbf{a}_1$ (see Fig. 9). We define $\mathbf{C}$, the vector that connects the two edges, and $\mathbf{C}' = \mathbf{C} + 2\mathbf{a}_2 - \mathbf{a}_1$ is the vector connecting $\boldsymbol{\beta}_1'$ and $\boldsymbol{\beta}_2'$, the lines of empty-site nearest neighbors to the edges $\boldsymbol{\beta}_1$ and $\boldsymbol{\beta}_2$.

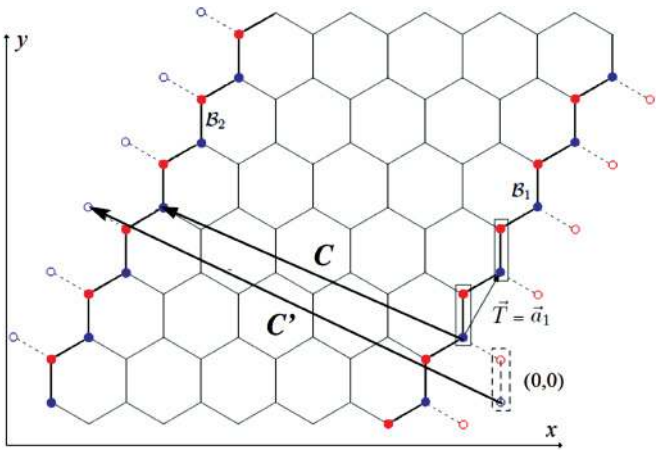

FIG. 10. (Color online) Schematic representation of a zigzag ribbon. The zigzag edge is obtained by translating the dimer A-B (represented by a rectangle) with the periodicity $\mathbf{T} = \mathbf{a}_1$. The two edges $\boldsymbol{\beta}_1$ and $\boldsymbol{\beta}_2$ are represented by thick lines. The first vacant sites outside of the ribbon where we impose the wave function to vanish are represented by circles. $\mathbf{C}$ is the vector of the Bravais lattice that connects two sites on both edges, and $\mathbf{C}'$ connects the first vacant site on one side of the ribbon to the first vacant site on the other side.

Noting $\Psi_{\mathbf{k}\pm} = (\Psi^A_{\mathbf{k}\pm},\Psi^B_{\mathbf{k}\pm})^T$, the Bloch state of momentum $\mathbf{k}$, we have

$$\Psi_{\mathbf{k},\pm}(\mathbf{r}) = \langle\mathbf{r}|\Psi_{\mathbf{k}\pm}\rangle \propto \frac{e^{i\mathbf{k}\cdot\mathbf{r}}}{\sqrt{2}}\begin{pmatrix} e^{-i\phi(\mathbf{k})} \\ \pm 1\end{pmatrix}. \tag{36}$$

Following the approach used for the one-dimensional chain of dimers of Sec. II B, we construct eigenstates of the ribbon as a linear combination Ψ of two Bloch states $\Psi_{\mathbf{k}\pm}$ and $\Psi_{\mathbf{k}'\pm}$ at the same energy. From Fig. 10, we see that the boundary conditions read

$$\Psi^A(\mathbf{C}' + \nu\mathbf{T}) = 0 \qquad [\text{on } \mathcal{B}_2'], \tag{37}$$

$$\Psi^B(\nu\mathbf{T}) = 0 \qquad [\text{on } \mathcal{B}_1'], \tag{38}$$

with $\nu \in \mathbb{Z}$.

The boundary condition Eq. (38) implies that the wave functions Ψ are combinations of the form $\Psi = \Psi_{\mathbf{k}} - \Psi_{\mathbf{k}'}$ with $\mathbf{k}\cdot\mathbf{T} = \mathbf{k}'\cdot\mathbf{T}$ (here $\mathbf{T} = \mathbf{a}_1$). Since we need $\epsilon_{\mathbf{k}} = \epsilon_{\mathbf{k}'}$, we have to consider momentum pairs $(\mathbf{k},\mathbf{k}')$ such that $(\mathbf{k}+\mathbf{k}')\cdot\mathbf{a}_2 = \mathbf{k}\cdot\mathbf{a}_1 = \mathbf{k}'\cdot\mathbf{a}_1$. For a given value of $k_\parallel$, it can be checked that this is satisfied if

$$\mathbf{k} = \mathbf{k}_\parallel + \mathbf{k}_\perp, \tag{39}$$

$$\mathbf{k}' = \mathbf{k}_\parallel - \mathbf{k}_\perp, \tag{40}$$

where we have introduced $\mathbf{k}_\parallel = k_\parallel\mathbf{e}_\parallel$ and $\mathbf{k}_\perp = k_\perp\mathbf{e}_\perp$. Note that $\mathbf{k}_\perp = 0$ or $\mathbf{k}_\perp = \mathbf{\Gamma}_\perp/2$ correspond to $\Psi_{\mathbf{k}} - \Psi_{\mathbf{k}'} \equiv 0$.

The boundary condition Eq. (38) then imposes

$$(\mathbf{k}-\mathbf{k}')\cdot\mathbf{C}' - (\phi(\mathbf{k}) - \phi(\mathbf{k}')) = 2\kappa\pi \tag{41}$$

(for integer κ) or, in term of the phase $\phi(k_\parallel,k_\perp) = \frac{1}{2}[\phi(\mathbf{k}_\parallel + \mathbf{k}_\perp) - \phi(\mathbf{k}_\parallel - \mathbf{k}_\perp)]$,

$$\mathbf{k}_\perp\cdot\mathbf{C}' - \phi(k_\parallel,k_\perp) = \kappa\pi, \tag{42}$$

which is the strict equivalent of the quantization condition (14) obtained for the 1D chain. We note, furthermore, that

$(\mathbf{\Gamma}_\perp \cdot \mathbf{C}') = 2\pi(M+1)$, with M the number of dimers in the transverse direction of the ribbon and, thus, half the number of bands. Using the same arguments as in Sec. II B, we see that the number of edge states depends on the value of $\phi(k_\parallel, \Gamma_\perp/2)$ and, more precisely, that the quantity

$$\left|\frac{\mathcal{Z}(k_\parallel)}{\pi}\right| = \left|\frac{1}{2\pi}\oint dk_\perp \frac{d\phi(k_\parallel,k_\perp)}{dk_\perp}\right| \tag{43}$$

gives the number of pairs of edge states (with opposite energies) for a given $k_\parallel$.

E. General orientation

We consider now graphene ribbons characterized by an arbitrary translation vector $\mathbf{T}(m,n)$. Based on similar arguments as in the previous section we conjecture that the relation between the Zak phase and the number of edge states holds in this general case. We then use this relation to predict the existence of edge states in graphene ribbons of general orientation. We also check that for every case for which edge states has been computed (numerically or otherwise) their appearance is correctly predicted by the Zak phase.

In Eq. (34), the phase $\phi(\mathbf{k})$ should be understood as a multivalued function. The single-valued function $\tilde{\phi}(\mathbf{k})$ corresponding to the restriction of $\phi(\mathbf{k})$ to the interval $[-\pi, +\pi]$ is displayed on Fig. 11. It shows lines of discontinuity connecting pairs of Dirac points. The location of the discontinuities (i.e., which Dirac points are connected by them) depends on the choice made for the unit-cell dimer A-B (oriented along the y axis in this paper; see Fig. 9). Therefore, the phase $\phi(\mathbf{k})$ is not invariant by a rotation of an angle $\pm 2\pi/3$.

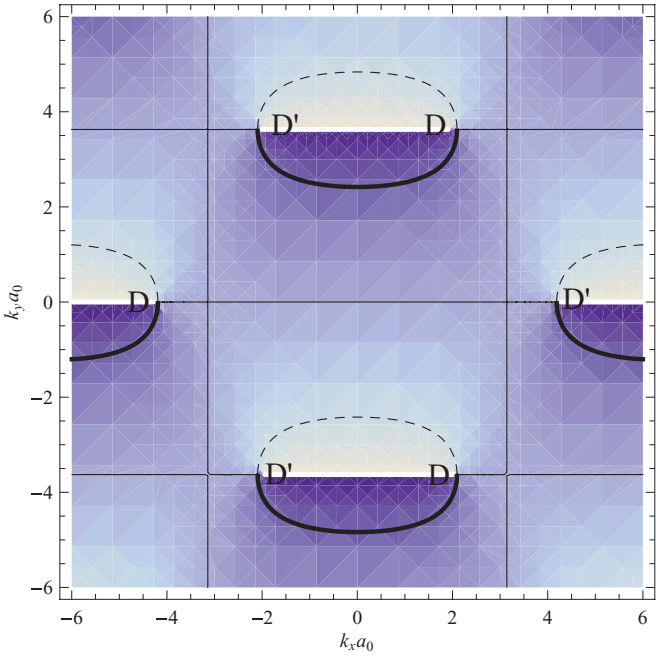

FIG. 11. (Color online) Density plot of the phase $\tilde{\phi}(\mathbf{k})$. The discontinuities of the phase are shown by horizontal white lines connecting pairs of Dirac points. These singularities separate the values $\tilde{\phi} = +\pi$ (light region) to the value $\tilde{\phi} = -\pi$ (dark region). Consequently, the only paths $\Gamma_\perp$ that contribute to a nonvanishing Zak phase are those that cross these singularities. The black lines, thick lines, and dashed lines represent the iso-$\tilde{\phi}$ lines, respectively, for $\tilde{\phi} = 0$, $\tilde{\phi} = -\pi/2$, and $+\pi/2$.

Let us start again by considering ribbons of period $\mathbf{T}(m,n)$ with coprime (m,n). The discontinuities of $\tilde{\phi}(\mathbf{k})$ are extremely convenient to determine the Zak phase since paths that lead to a nonvanishing Zak phase necessarily cross a discontinuity line. Actually, the Zak phase $\mathcal{Z}_{(m,n)}(k_\parallel)$ is given by the number of discontinuities $d(k_\parallel)$ intersected by the path $\mathcal{P}_{(m,n)}(k_\parallel) = [\mathbf{k}_\parallel, \mathbf{k}_\parallel + \mathbf{\Gamma}_\perp]$ along which $\mathcal{Z}_{(m,n)}(k_\parallel)$ is computed, that is,

$$\mathcal{Z}(k_\parallel) = \pm\pi\ d(k_\parallel). \tag{44}$$

In other words, $d(k_\parallel)$ is just the number of pairs of edge states (of opposite energies) for a given $k_\parallel$.

These considerations make it possible to compute graphically the Zak phase in a rather straightforward way. For a given choice of edge characterized by the vector $\mathbf{T}(m,n) = m\mathbf{a}_1 + n\mathbf{a}_2$, we first represent the vector $\mathbf{\Gamma}_\perp(m,n) = n\mathbf{a}_1^* - m\mathbf{a}_2^*$ [Eq. (32)]. This is done in Fig. 12, where we plot the vectors $\mathbf{\Gamma}_\perp(m,n)$ from the left extremity of the discontinuity (0,0) to the left extremity of the discontinuity $(n, -m)$. Next, in Fig. 13, we translate perpendicularly $\mathbf{\Gamma}_\perp$ until the left extremity of an another discontinuity is reached (dashed line), which gives $\mathbf{\Gamma}_\parallel(m,n)$. The rectangle defined by $\mathbf{\Gamma}_\perp$ and $\mathbf{\Gamma}_\parallel$ is the Brillouin zone we want to associate with the ribbon. For a given value of the momentum $k_\parallel$, $\mathcal{Z}(k_\parallel)$ is then deduced from Eq. (44) by simply counting the number of intersections of the segment $[\mathbf{k}_\parallel, \mathbf{k}_\parallel + \mathbf{\Gamma}_\perp]$ with the discontinuity lines of $\tilde{\phi}(\mathbf{k})$.

If m and n are not coprime, as, for instance, in Fig. 13(d), $\mathbf{\Gamma}_\parallel(m,n)$ and $\mathbf{\Gamma}_\perp(m,n)$ cannot be obtained in this way as they do not define a Brillouin zone. Writing, however, $(m,n) = l(\tilde{m},\tilde{n})$ with $(\tilde{m},\tilde{n})$ coprime, the Brillouin zone corresponding to

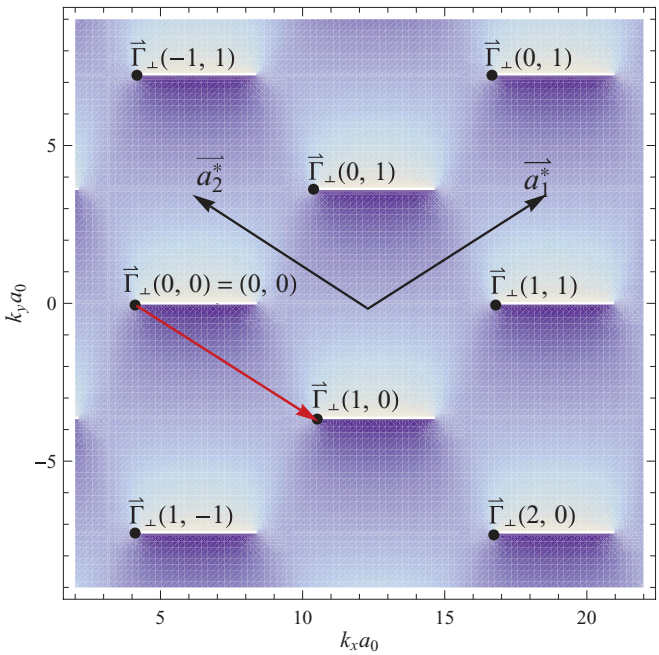

FIG. 12. (Color online) On top of the density plot of the phase $\tilde{\phi}(\mathbf{k})$, we have represented several values of the vector $\mathbf{\Gamma}_\perp(m,n) = n\mathbf{a}_1^* - m\mathbf{a}_2^*$. The left extremity of a discontinuity of $\tilde{\phi}(\mathbf{k})$ is taken as the origin. We have explicitly plotted the vector $\mathbf{\Gamma}_\perp(1,0)$ as an example.

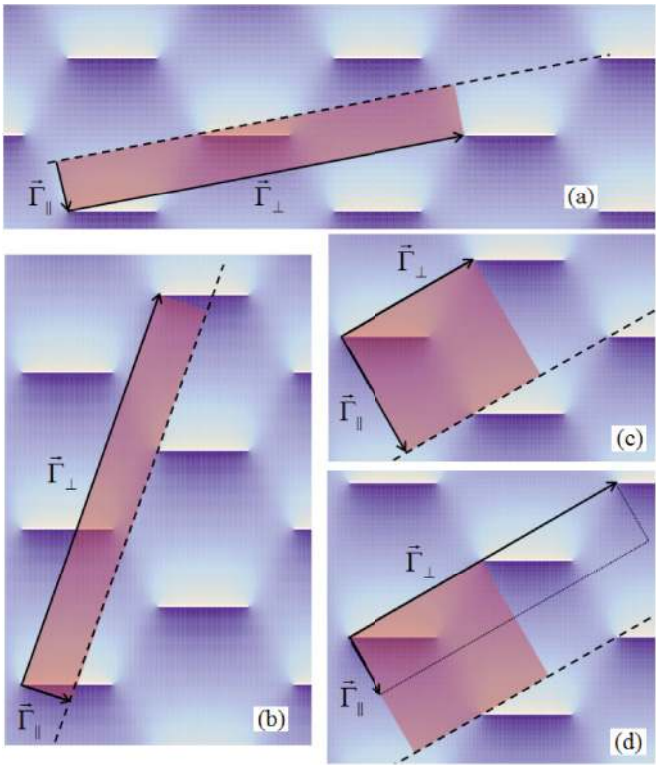

FIG. 13. (Color online) Surfaces $|\mathbf{\Gamma}_\parallel \wedge \mathbf{\Gamma}_\perp|$ associated with different ribbon vectors $\mathbf{T}(m,n)$. $\mathbf{\Gamma}_\perp$ is obtained as $\mathbf{\Gamma}_\perp(m,n) = n\mathbf{a}_1^* - m\mathbf{a}_2^* = (n,-m)$; see text for the construction of $\mathbf{\Gamma}_\parallel$. (a) $\mathbf{\Gamma}_\perp(m = 1,n = 2) = (2,-1)$, (b) $\mathbf{\Gamma}_\perp(-2,3) = (3,2)$, and (c) $\mathbf{\Gamma}_\perp(0,1) = (1,0)$. In these three cases, m and n are coprime, and the surfaces $|\mathbf{\Gamma}_\parallel \wedge \mathbf{\Gamma}_\perp|$ represented by a shaded rectangles are Brillouin zones. (d) For $\mathbf{T}(0,2)$ the surface obtained by $\mathbf{\Gamma}_\parallel$ and $\mathbf{\Gamma}_\perp$ is not a Brillouin zone because m and n are not coprime. The corresponding Brillouin zone (shaded rectangle) is given by $\mathbf{\Gamma}_\perp(0,1) = \mathbf{\Gamma}_\perp(0,2)/2$ and $\mathbf{\Gamma}_\parallel(1,0) = 2\mathbf{\Gamma}_\parallel(2,0)$.

$(\tilde{m},\tilde{n})$ can be constructed as above, and one has simply $\mathbf{\Gamma}_\parallel(m,n) = \tilde{\mathbf{\Gamma}}_\parallel(\tilde{m},\tilde{n})/l$ and $\mathbf{\Gamma}_\perp(m,n) = l\tilde{\mathbf{\Gamma}}_\perp(\tilde{m},\tilde{n})$, which basically amounts to a folding of $\tilde{\mathbf{\Gamma}}_\parallel$ by a factor l. For a given value of $k_\parallel$, the Zak phase in then given by Eq. (35).

F. Range of existence and density of edge states

In this section we derive the range $\Delta k_\parallel$ for which edge states exist, as well as the density of edge states for arbitrary boundary conditions thanks to the bulk-edge correspondence in terms of the Zak phase.

In the last section, we showed that the number of pairs of edge states for a given value of $k_\parallel$ is given by the number $d(k_\parallel)$ of crossings between the path $\mathcal{P}_{(m,n)}(k_\parallel)$ and the discontinuities of $\tilde{\phi}(\mathbf{k})$. Since a Brillouin zone always contains exactly one line of discontinuities, the total range

$$\Delta k_\parallel \equiv \int_0^{2\pi/|\mathbf{T}|} d(k_\parallel)dk_\parallel \tag{45}$$

over which the ribbon exhibits edge states, is obtained by projecting the line of discontinuities onto the $k_\parallel$ axis, as illustrated in Fig. 14. This leads to

$$\Delta k_\parallel = \frac{4\pi}{3a_0}|\sin\theta|, \tag{46}$$

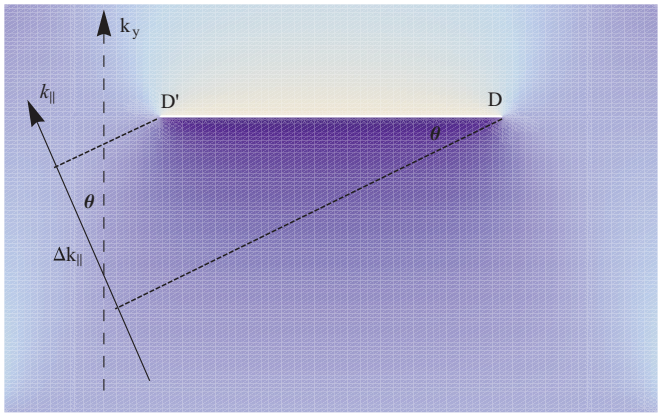

FIG. 14. (Color online) Projection of the discontinuity of $\tilde{\phi}(\mathbf{k})$ onto the $k_\parallel$ axis. This projection gives the range $\Delta k_\parallel$ for the existence of edge states.

where θ is the angle between the direction $\mathbf{T}$ of the ribbon and the vertical axis y of the dimers [see Fig. 9 and Eq. (30)]. Therefore, there is no edge state for edges parallel to the armchair edge ($\theta = 0$) and $\Delta k_\parallel$ is maximum and equal to $4\pi/3a_0$ for bearded edges.[19,20]

Then, from Eq. (30) we have the relation between the range $\Delta k_\parallel$ of existence of edge states in graphene and the integers (m,n) characterizing the edge:

$$\Delta k_\parallel(m,n) = \frac{2\pi}{3a_0}\frac{|n-m|}{\sqrt{n^2+m^2+nm}}. \tag{47}$$

We note that $\Delta k_\parallel(m,n) = \Delta k_\parallel(lm,ln)$, which means that $\mathbf{T}(m,n)$ and $l\mathbf{T}(m,n)$ support the same number of localized states. A relevant quantity to study is the ratio $\mathcal{R} \equiv \Delta k_\parallel/|\mathbf{\Gamma}_\parallel| = \Delta k_\parallel|\mathbf{T}|/(2\pi)$, which gives the relative range of the 1D Brillouin zone where edge states exist. We find

$$\mathcal{R} = \frac{|n-m|}{3}. \tag{48}$$

We now comment on Eqs. (47) and (48). First, we apply these formulas to several types of edges as listed in Table I.

The three general types of edges mentioned in this table represent a zigzag profile extending over, respectively, three, five, and eight unit cells followed by an armchair defect [see, for example, Fig. 1 for the case (1,5)]. These results are in good agreement with the size of the edge states energy bands obtained by numerical tight-binding calculations in different previous works.[2,3,14,21–23] We also note that in the limit $|n| \gg$

TABLE I. Applications of Eqs. (47) and (48) for some edge geometries studied in previous works.

	(m,n)	$\Delta k_\parallel$	$\mathcal{R}$
Armchair	(1,1)	0	0
Zigzag	(1,0)	$2\pi/3a_0$	1/3
Bearded zigzag	(1, −1)	$4\pi/3a_0$	2/3
Bearded armchair	(2, −1)	$2\pi/\sqrt{3}a_0$	1
	(1,3)	$4\pi/3\sqrt{13}a_0$	2/3
General types	(1,5)	$2\pi/3\sqrt{31}a_0$	4/3
	(1,8)	$14\pi/15\sqrt{3}a_0$	7/3

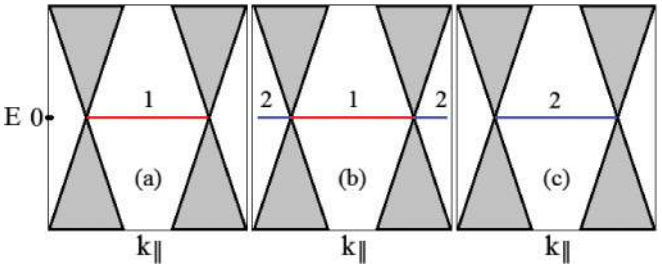

FIG. 15. (Color online) Schematic band structures of graphene ribbons that exhibit edge states. Edge states are represented as zero-energy flat bands as expected in the large width limit within the tight-binding model (assuming the chiral symmetry is preserved). The number of pairs of edge states is indicated on the three figures (a), (b) and (c). In Fig. (a), the parameter $\mathcal{R} < 1$ and in Fig. (b) $\mathcal{R} > 1$. Our analysis based on the Zak phase predicts that the configuration (c) is not allowed.

$|m|$ (or the other way), we recover $\Delta k_\parallel \to 2\pi/3a_0$ which is the expected result for the zigzag edge.

Equations (47) and (48) directly lead to the important result that edge states exist for most types of ribbons with a periodic pattern, which is in agreement with a previous analytical approach within the Dirac framework.[24] More precisely, we find that there is no edge state if and only if $n = m$. As already mentioned, this class of ribbons includes all the vectors $\mathbf{T}$ parallel to the y axis of the dimers A-B [see, for instance, the case (3,3) displayed in Fig. 1. Similar ribbons have been synthesized recently].[29] The well-known particular armchair case corresponds to the smallest $|\mathbf{T}|$ that obeys this condition.

The case $\mathcal{R} \geqslant 1$ also deserves some attention. It implies that two or more pairs of localized states may correspond to the same $k_\parallel$. This situation happens when, as illustrated in the example of Fig. 13(b), several discontinuities are intersected by the path $\mathcal{P}_{(m,n)}(k_\parallel)$. Such a situation is automatically achieved for m and n coprime when $\theta(m,n) > \theta(4,1) = \arctan(\sqrt{3}/5)$. Moreover, by construction, the projection of the line of discontinuity of $\tilde{\phi}$ spans $\mathcal{R}$ times the Brillouin zone, which implies that the number of localized states cannot differ by more than one unit for any two $k_\parallel$ (see Fig. 15).

Therefore, for m and n coprime, there is either $[\mathcal{R}]$ or $[\mathcal{R}] + 1$ edge states for each $k_\parallel$ ($[x]$ is the floor function). In the particular case where $\mathcal{R}$ is an integer there are exactly $\mathcal{R}$ edge states for each $k_\parallel$.

Finally, we can define the quantity $\rho = \mathcal{R}/|\mathbf{T}|$ which corresponds to the "density of edge states per unit length" introduced by Akhmerov and Beenakker. We get

$$\rho = \frac{\Delta k_\parallel}{2\pi} = \frac{1}{3a_0}\frac{|n-m|}{\sqrt{n^2+m^2+nm}}, \tag{49}$$

which was first obtained in Ref. 24 for "minimal boundary conditions" (m and n have the same sign) by a different method.

IV. EMERGENCE AND DESTRUCTION OF EDGE STATES: A TOPOLOGICAL APPROACH

In this section, we generalize the formula (47) for nonequal hopping parameters $t_1 \neq t_2 \neq t_3$ and establish a criterion for the existence of edge states for an anisotropic honeycomb lattice. We show that the manipulation of these parameters leads to a topological transition described in terms of Zak phase that affects the range $\Delta k_\parallel$ of existence of edge states. We stress that breaking the isotropy of the hopping parameters preserves the chiral symmetry, and, therefore, the topological character of the Zak phase. As a consequence the analysis developed in the previous section generalizes straightforwardly to the case considered below.

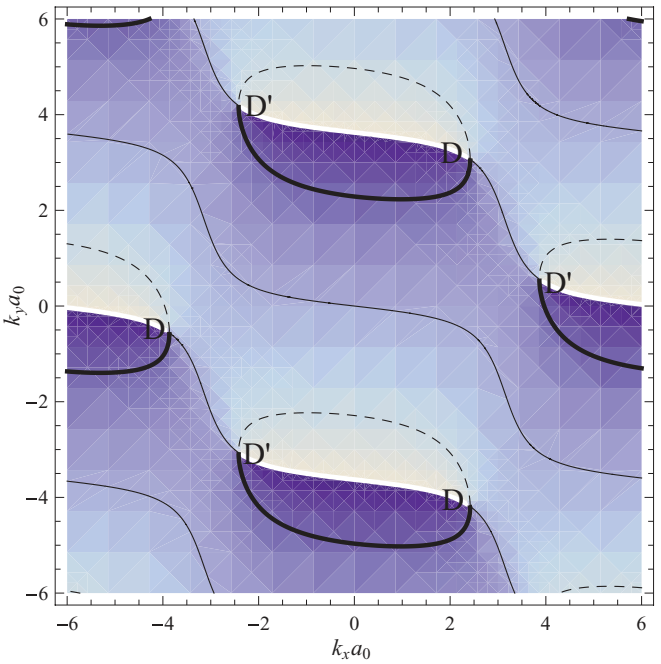

FIG. 16. (Color online) Density plot of the phase $\tilde{\phi}(\mathbf{k})$ for $t_2 = 1.5t_1 = 1.5t_3$. The discontinuities of the phase are shown by curved white lines that pair the Dirac points. The black lines, thick lines, and dashed lines represent the iso-$\tilde{\phi}$ lines, respectively, for $\tilde{\phi} = 0$, $\tilde{\phi} = -\pi/2$, and $+\pi/2$.

A. Effect of an anisotropy on the existence of edge states

Several previous works dealing with the tight-binding model in the honeycomb lattice showed that the Dirac points move when modifying the ratio of the parameters t_i/t_j.[30–33] As the lines of discontinuities of $\tilde{\phi}(\mathbf{k})$ connect pairs of Dirac points, the modification of the ratio t_i/t_j changes the Zak phase and, therefore, leads to new ranges $\Delta k_\parallel$ of existence of edge states. This is clearly shown in Fig. 16.

To determine these new ranges, we, first, have to specify the position of the Dirac points for any t_i. To a vector of the reciprocal lattice, they are given by

$$\begin{aligned}\mathbf{D} &= -\frac{\pi - d_1}{2\pi}\mathbf{a}_1^* + \frac{\pi - d_2}{2\pi}\mathbf{a}_2^*,\\ \mathbf{D}' &= \frac{\pi - d_1}{2\pi}\mathbf{a}_1^* - \frac{\pi - d_2}{2\pi}\mathbf{a}_2^*,\end{aligned} \tag{50}$$

with

$$\begin{aligned}d_1 &= \mathbb{R}\mathrm{e}\left[\arccos\left(\frac{t_3^2 + t_2^2 - t_1^2}{2t_2t_3}\right)\right],\\ d_2 &= \mathbb{R}\mathrm{e}\left[\arccos\left(\frac{t_3^2 + t_1^2 - t_2^2}{2t_1t_3}\right)\right],\end{aligned} \tag{51}$$

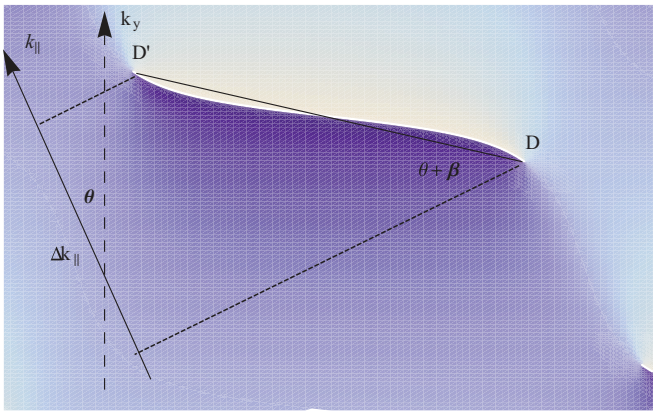

FIG. 17. (Color online) Projection of the discontinuity line of $\tilde{\phi}(\mathbf{k})$ onto the $k_\parallel$ axis. The asymmetry of the hopping induces a modification of the discontinuity locations as compared with Fig. 14.

where $\mathbb{R}\mathrm{e}(x)$ takes the real part of x. The Cartesian coordinates od the Dirac points $\mathbf{D}^{(\prime)} = (D_x^{(\prime)}, D_y^{(\prime)})$ are given by

$$\begin{aligned}\mathbf{D} &= [(d_1 + d_2 - 2\pi)/a_0, (d_1 - d_2)/\sqrt{3}a_0] \\ \mathbf{D}' &= [(-d_1 - d_2 + 2\pi)/a_0, (d_2 - d_1)/\sqrt{3}a_0].\end{aligned} \tag{52}$$

Then, since the Dirac points $\mathbf{D}^{(\prime)}$ are not located anymore at the corner $\mathbf{K}^{(\prime)}$ of the Brillouin zone, the range $\Delta k_\parallel$ of existence of edge states is modified as

$$\Delta k_\parallel = |\mathbf{D} - \mathbf{D}'||\sin(\theta + \beta)|, \tag{53}$$

where β is the angle between the line $[\mathbf{D}'\mathbf{D}]$ and the k_x axis (see Fig. 17), which is then given by

$$\begin{aligned}\cos\beta &= 2\frac{2\pi/a_0 - D'_x}{|\mathbf{D} - \mathbf{D}'|}, \\ \sin\beta &= 2\frac{D'_y}{|\mathbf{D} - \mathbf{D}'|}.\end{aligned} \tag{54}$$

Using Eqs. (30) and (54), the range for the edge states reads:

$$\Delta k_\parallel = \frac{\left|(n-m)\left(\frac{2\pi}{a_0} - D'_x\right) + \sqrt{3}(n+m)D'_y\right|}{\sqrt{n^2 + m^2 + mn}}. \tag{55}$$

Next, by using the expression of the positions D'_x and D'_y given in Eq. (52), one finds:

$$\Delta k_\parallel = \frac{2|nd_2 - md_1|}{a_0\sqrt{n^2 + m^2 + nm}} \tag{56}$$

as well as

$$\mathcal{R} = \frac{|nd_2 - md_1|}{\pi}, \tag{57}$$

where d_1 and d_2 are given by Eqs. (51). These results give a criterion for the existence of edge states that links the anisotropy of the hopping parameters encoded in d_1 and d_2 with the nature of the edge characterized by (m,n). In the isotropic case, we have $d_1 = d_2 = \pi/3$, and we recover the result [Eq. (47)] discussed in the previous section. Equation (56) means that an edge state exists in graphenelike structures if $|nd_1 - md_2| \neq 0$.

An interesting consequence is that, for a given type of ribbon, edge states can emerge or collapse when an anisotropy is applied. For instance, edge states can emerge for armchairlike boundary conditions ($m = n$) when either $t_1/t_3 \neq 1$ or $t_2/t_3 \neq 1$ (see Refs. 26, 34, and 35 for the case $n = m = 1$). This is clearly displayed in Fig. 18.

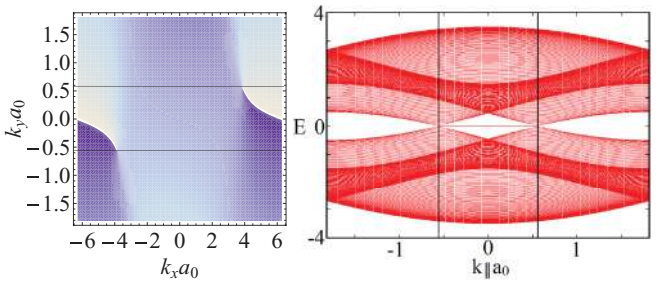

FIG. 18. (Color online) (Left) Density plot of the phase $\tilde{\phi}(\mathbf{k})$ for $t_1 = 1$, $t_2 = 1.5$, and $t_3 = 1$ represented in the Brillouin zone corresponding to armchair edges. The two horizontal lines delimit the region where $\mathcal{Z}(k_\parallel) = \pi$. (Right) Band structure of an armchair ribbon with the same hopping parameters. In this case, $k_\parallel = k_y$. The two vertical lines delimit the same range as in the left panel, which is such that edge states at zero energy, clearly separated from the bulk bands, have emerged.

In the same way, edge states can collapse by manipulating the asymmetry of the hopping in such a way that $|nd_1 - md_2| = 0$.

B. Merging of Dirac points and edge states

As one increases the anisotropy of the system, for instance, by modifying one of the ratio t_i/t_j, one may eventually reach a point where $t_1 = t_2 + t_3$ (or the equivalent up to a cyclic permutation of the indices). From Eq. (51), this condition implies that d_1 and d_2 take the values 0 or π, which, from Eq. (52), corresponds to *a merging of the Dirac points*. By increasing further the anisotropy, a gap opens at the merging point. This merging is a topological transition since the Berry phases $\pm\pi$ associated to the two Dirac points annihilate at the transition.[31,33]

This topological transition is a bulk property and is, thus, independent of the orientation of the anisotropy. On the other hand, the existence of edge states at the merging transition and beyond depends on the orientation of the ribbon with respect to this anisotropy, and this information is still contained in the Zak phase. Indeed, the anisotropy of the hopping parameters controls the size and the location of the lines of discontinuities of $\tilde{\phi}(\mathbf{k})$. It is, therefore, essential to distinguish which pair of Dirac points merges. There are three possibilities as follows:

(i) $t_3 \geqslant t_1 + t_2$

In this configuration, the Dirac points that merge are the end points of the same discontinuity line. The discontinuities then disapper at the merging point ($t_1 + t_2 = t_3$) and the Zak phase vanishes. This leads to

$$\mathcal{R} = 0, \tag{58}$$

whatever m and n (see top panel of Fig. 19), implying that edge states never exist in this case. As an illustration, we plot in Fig. 19 the band structure of a zigzag ribbon exactly at the merge point: The zero energy edge states[2] of the isotropic case have collapsed because the Zak phase is zero for all $k_\parallel$.

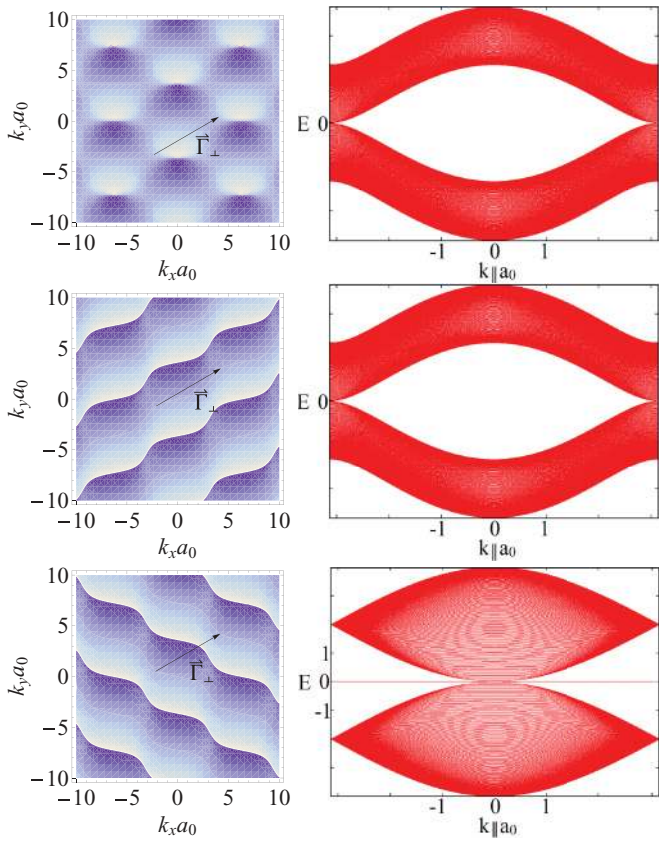

FIG. 19. (Color online) Density plot of the phases $\tilde{\phi}(\mathbf{k})$ at the merging of the Dirac points, and the band structure for a zigzag ribbon with $\theta = \pi/6$ [that is, $\mathbf{T}(m = 0,n = 1) \to \mathbf{\Gamma}_\perp(m = 0,n = 1) = (1,0)$]. (Top) $t_1 = 1$, $t_2 = 1$, and $t_3 = 2$; (center) $t_1 = 2$, $t_2 = 1$, and $t_3 = 1$; (bottom) $t_1 = 1$, $t_2 = 2$, and $t_3 = 1$. The scale is given in units of $1/a_0$.

The situation differs totally when the two merging Dirac points are attached to two distinct discontinuity lines, which occurs when $t_1 - t_2 = \pm t_3$. In this case, the two discontinuity lines themselves merge, implying that $\mathcal{R}$ is an integer, as we discuss now.

(ii) $t_1 \geqslant t_2 + t_3$

In this case we have $d_2 = 0$ and $d_1 = \pi$, which leads to

$$\mathcal{R} = |m| \tag{59}$$

for all n. For instance, there is no edge state for zigzag edge at $\theta = +\pi/6$ (see center panels of Fig. 19), but there is one over the whole ribbon Brillouin zone for armchair edges and for zigzag edges at $\theta = -\pi/6$. We note that the existence of edge states now depends only on the orientation of the edge given by θ but no longer on $k_\parallel$.

(iii) $t_2 \geqslant t_1 + t_3$

In this case $d_1 = 0$ and $d_2 = \pi$ and we find

$$\mathcal{R} = |n|, \tag{60}$$

whatever the value of m. Of course, this case is equivalent to the one discussed previously with the substitution $m \leftrightarrow n$, that is, $\theta \to -\theta$. The phase $\tilde{\phi}(\mathbf{k})$ and the corresponding band structure for zigzag ribbons at $\theta = +\pi/6$ are represented in Fig. 19 (bottom panels).

In summary, we note that in all three cases, at the merging point, the Zak phase becomes independent of $k_\parallel$ and remains unchanged in the gapped phase. This implies that at the merging transition and beyond, $\mathcal{R}$ is, necessarily, an integer. This is obvious from Figs. 19: the merging of the Dirac points implies either a disparition of the discontinuity lines or their transformation into an infinite line.

V. CONCLUSION

In this paper, we have investigated the correspondence between the Zak phase and the existence of edge states for arbitrarily oriented graphene ribbons with a large class of edge shapes. We have proposed a definite prescription to compute the Zak phase in order to predict the number of edge states. The approach we have developed consists in constructing the appropriate 2D Brillouin zone associated with the vector $\mathbf{T}(m,n)$ that defines the edge. The Zak phase $\mathcal{Z}(k_\parallel)$ giving the number of edge states for each $k_\parallel$ is then directly obtained by integrating the Berry connection along a path fixed by $\mathbf{T}(m,n)$ and $k_\parallel$ in this 2D Brillouin zone.

We stress that this bulk-edge correspondence is, beyond the 1D chain of dimers case, only rigorously proven here for zigzag edges. It is, therefore, so far a conjecture for the class of edges we have defined. This conjecture is, however, supported by the fact that it reproduces all the known previous results obtained (numerically or otherwise) in the literature for various specific types of edges.[2,3,14,21–23]

In practice, the value of the integral defining the Zak phase is easily obtained graphically. Our approach, therefore, requires no sophisticated formalism or calculation and gives an elegant understanding of the origin of the edge-dependent edge states in terms of a topological bulk quantity. In particular, it provides a simple understanding of the appearance and disappearance of edge states by manipulating the anisotropy of the tight-binding hopping parameters. Such a manipulation may be induced in graphene by applying an uniaxial stress or bending of the sheet[36] or in photonic crystals which mimic the same physics by changing the distance between the confining mirrors.[6] We finish with a few comments concerning the connection between Zak phase and edge states.

First, this bulk-edge correspondence differs from the ones in quantum Hall systems[37–40] or $\mathbb{Z}_2$ topological insulators[40,41] since here the existence of edge states precisely depends on the orientation of the edge. This difference with the usual bulk topological numbers originates from the fact that the Zak phase is a 1D (rather than 2D) integral of the Berry connection.

Second, we stress that within our approach, the vector $\mathbf{T}(m,n)$ defining the periodicity of the ribbon entirely determine the Zak phase. As many different shapes may correspond to the same vector $\mathbf{T}(m,n)$, the Zak phase and, therefore, the number of edge states are expected to be independent of the variation of the edge geometries as long as they correspond to the same $\mathbf{T}(m,n)$.[42]

Finally, our description of edge states in terms of the Zak phase is *a priori* not restricted to graphene but, in principle, should be also applicable to other 2D systems like d-wave superconductors,[14] a square lattice with half a quantum flux per unit cell,[35] or bilayer graphene,[17] for instance.

ACKNOWLEDGMENTS

We acknowledge useful discussions with J.-N Fuchs, M. Büttiker, J. Li, C. Bena and L. Bilteanu. This work is supported by the NANOSIMGRAPHENE Project No. ANR-09-NANO-016-01 of ANR/P3N2009. In Geneva, P.D. was supported by the European Marie Curie ITN NanoCTM.

APPENDIX: CONSTRUCTION OF THE BRILLOUIN ZONE

In this Appendix, we give a brief reminder of the reason why the vectors $\mathbf{\Gamma}_{\parallel}$ and $\mathbf{\Gamma}_{\perp}$ defined by Eqs. (31) and (32) actually generate a Brillouin zone when n and m are coprime integers.

This latter condition indeed implies that one can find two integers (m',n') such that $mn' - nm' = 1$, in which case the couple of vector $(\mathbf{T},\mathbf{N})$, with $\mathbf{N} = m'\mathbf{a}_1 + n'\mathbf{a}_2$, form a basis of the Bravais lattice. The choice of (m',n'), and, thus, of $\mathbf{N}$, is not unique, but this is irrelevant for our purpose.

From $(\mathbf{T},\mathbf{N})$, one deduce a basis $(\mathbf{\Gamma}_N,\mathbf{\Gamma}_{\perp})$ of the reciprocal lattice,

$$\mathbf{\Gamma}_N = n'\mathbf{a}_1^* - m'\mathbf{a}_2^*, \tag{A1}$$

$$\mathbf{\Gamma}_{\perp} = n\mathbf{a}_1^* - m\mathbf{a}_2^*, \tag{A2}$$

which is such that $\mathbf{\Gamma}_{\perp} \perp \mathbf{T}$. A Brillouin zone can, thus, be obtained from the parallelogram generated by $(\mathbf{\Gamma}_N,\mathbf{\Gamma}_{\perp})$. More generally, however, any vector $\mathbf{\Gamma}$ such that $(\mathbf{\Gamma} - \mathbf{\Gamma}_N) \parallel \mathbf{\Gamma}_{\perp}$ is such that the parallelogram generated by $(\mathbf{\Gamma},\mathbf{\Gamma}_{\perp})$ is a Brillouin zone. A natural choice is to take for $\mathbf{\Gamma}$ the vector $\mathbf{\Gamma}_{\parallel}$ that is parallel to $\mathbf{T}$ (and, thus, orthogonal to $\mathbf{\Gamma}_{\perp}$). Since $\mathbf{T}\cdot\mathbf{\Gamma}_N = 2\pi(mn' - nm') = 2\pi$, one has $|\mathbf{\Gamma}_{\parallel}| = 2\pi/|\mathbf{T}|$, which is nothing but the size of the (1D) Brillouin zone of the ribbon.

[1] A. Geim and K. Novoselov, Nat. Mater. **6**, 183 (2007).
[2] M. Fujita, K. Wakabayashi, K. Nakada, and K. Kusakabe, J. Phys. Soc. Jpn. **65**, 1920 (1996).
[3] K. Nakada, M. Fujita, G. Dresselhaus, and M. S. Dresselhaus, Phys. Rev. B **54**, 17954 (1996).
[4] Y. Kobayashi, K. I. Fului, T. Enoki, K. Kusakabe, and Y. Kaburagi, Phys. Rev. B **71**, 193406 (2005).
[5] Y. Niimi, T. Matsui, H. Kambara, K. Tagami, M. Tsukada, and H. Fukuyama, Phys. Rev. B **73**, 085421 (2006).
[6] U. Kuhl, S. Barkhofen, T. Tudorovskiy, H.-J. Stockmann, T. Hossain, L. de Forges de Parny, and F. Mortessagne, Phys. Rev. B **82**, 094308 (2010).
[7] Y.-W. Son, M. L. Cohen, and S. G. Louie, Nature **444**, 347 (2006).
[8] O. V. Yazyev and M. I. Katsnelson, Phys. Rev. Lett. **100**, 047209 (2008).
[9] B. I. Halperin, Phys. Rev. B **25**, 2189 (1982).
[10] M. Büttiker, Phys. Rev. B **38**, 9375 (1988).
[11] B. A. Bernevig, T. A. Hughes, and S.-C. Zhang, Science **314**, 1757 (2006).
[12] M. Konig, H. Buhmann, L. W. Molenkamp, T. Hughes, C.-X. Liu, X.-L. Qi, and S.-C. Zhang, J. Phys. Soc. Jpn. **77**, 031007 (2008).
[13] D. J. Thouless, M. Kohmoto, M. P. Nightingale, and M. den Nij, Phys. Rev. Lett. **49**, 405 (1982).
[14] S. Ryu and Y. Hatsugai, Phys. Rev. Lett. **89**, 077002 (2002).
[15] R. Mong and V. Shivamoggi, Phys. Rev. B **83**, 125109 (2011).
[16] K. Sasaki, K. Wakabayashi, and T. Enoki, New J. Phys. **12**, 083023 (2010).
[17] J. Li, A. F. Morpurgo, M. Büttiker, and I. Martin, Phys. Rev. B **82**, 245404 (2010).
[18] T. T. Heikkilä, N. B. Kopnin, and G. E. Volovik, Pis'ma Zh. Eksp. Teor. Fiz. **94**, 252 (2011).
[19] D. J. Klein and L. Bytautas, J. Phys. Chem. A **103**, 5196 (1999).
[20] Z. Liu, K. Suenaga, P. J. F. Harris, and S. Iijima, Phys. Rev. Lett. **102**, 015501 (2009).
[21] K. Wakabayashi, Y. Takane, M. Yamamoto, and M. Sigrist, Carbon **47**, 124 (2009).
[22] K. Wakabayashi, S. Okada, R. Tomita, S. Fujimoto, and Y. Natsume, J. Phys. Soc. Jpn. **79**, 034706 (2010).
[23] W. Jaskolski, A. Ayuela, M. Pelc, H. Santos, and L. Chico, Phys. Rev. B **83**, 235424 (2011).
[24] A. R. Akhmerov and C. W. J. Beenakker, Phys. Rev. B **77**, 085423 (2008).
[25] J. Zak, Phys. Rev. Lett. **62**, 2747 (1989).
[26] H. Dahal, Z. Hu, N. Sinitsyn, K. Yang, and A. Balatsky, Phys. Rev. B **81**, 155406 (2010).
[27] When M is finite, there is a finite range of parameters $1 - 1/(M + 1) < t'/t < 1$, for which there are no edge states (M bulk states), although the Zak phase is π.
[28] The energy of the edge states is zero only when the width of the system is larger than the localization length, otherwise the edge states at each edge hybridize and the resulting energy is not zero.
[29] J. Cai *et al.*, Nat. Lett. **466**, 470 (2010).
[30] Y. Hasegawa, R. Konno, H. Nakano, and M. Kohmoto, Phys. Rev. B **74**, 033413 (2006).
[31] P. Dietl, F. Piéchon, and G. Montambaux, Phys. Rev. Lett. **100**, 236405 (2008).
[32] B. Wunsch, F. Guinea, and F. Sols, New J. Phys. **10**, 103027 (2008).
[33] G. Montambaux, F. Piéchon, J.-N. Fuchs, and M.-O. Goerbig, Eur. Phys. J. B **72**, 509 (2009).
[34] M. Kohmoto and Y. Hasegawa, Phys. Rev. B **76**, 205402 (2007).
[35] P. Delplace, Ph.D. thesis, Université Paris-Sud XI, 2010.
[36] L. Pauling, Proc. Natl. Acad. Sci. USA **56**, 1646 (1966).
[37] Y. Hatsugai, Phys. Rev. B **48**, 11851 (1993).
[38] Y. Hatsugai, Phys. Rev. Lett. **71**, 3697 (1993).
[39] N. Hao, P. Zhang, Z. Wang, W. Zhang, and Y. Wang, Phys. Rev. B **78**, 075438 (2008).
[40] X.-L. Qi, Y.-S. Wu, and S.-C. Zhang, Phys. Rev. B **74**, 045125 (2006).
[41] Z. Wang, N. Hao, and P. Zhang, Phys. Rev. B **80**, 115420 (2009).
[42] Preliminary numerical results seem to confirm this prediction (L. Bilteanu and C. Bena, private communication).